

# Robust PCA Unrolling Network for Super-Resolution Vessel Extraction in X-Ray Coronary Angiography

Binjie Qin<sup>1</sup>, Member, IEEE, Haohao Mao<sup>1</sup>, Yiming Liu<sup>1</sup>, Jun Zhao<sup>1</sup>, Member, IEEE, Yisong Lv<sup>1</sup>, Yueqi Zhu, Song Ding, and Xu Chen<sup>2</sup>

**Abstract**—Although robust PCA has been increasingly adopted to extract vessels from X-ray coronary angiography (XCA) images, challenging problems such as inefficient vessel-sparsity modelling, noisy and dynamic background artefacts, and high computational cost still remain unsolved. Therefore, we propose a novel robust PCA unrolling network with sparse feature selection for super-resolution XCA vessel imaging. Being embedded within a patch-wise spatiotemporal super-resolution framework that is built upon a pooling layer and a convolutional long short-term memory network, the proposed network can not only gradually prune complex vessel-like artefacts and noisy backgrounds in XCA during network training but also iteratively learn and select the high-level spatiotemporal semantic information of moving contrast agents flowing in the XCA-imaged vessels. The experimental results show that the proposed method significantly outperforms state-of-the-art methods, especially in the imaging of the vessel network and its distal vessels, by restoring the intensity and geometry profiles of heterogeneous vessels against complex and dynamic backgrounds. The source code is available at <https://github.com/Binjie-Qin/RPCA-UNet>

**Index Terms**—Algorithm unrolling, RPCA unrolling network, X-ray coronary angiography, vessel extraction, sparse feature selection, super-resolution.

Manuscript received 14 March 2022; revised 9 May 2022; accepted 21 May 2022. Date of publication 23 May 2022; date of current version 27 October 2022. This work was supported in part by the Science and Technology Commission of Shanghai Municipality under Grant 19dz1200500 and Grant 19411951507; in part by the National Natural Science Foundation of China under Grant 61271320 and Grant 82070477; in part by the Shanghai Shenkang Hospital Development Center under Grant SHDC12019-12; and in part by the Interdisciplinary Program of Shanghai Jiao Tong University under Grant ZH2018ZDA19, Grant YG2021QN122, and Grant YG2021QN99. (Corresponding author: Binjie Qin.)

Binjie Qin, Haohao Mao, Yiming Liu, and Jun Zhao are with the School of Biomedical Engineering, Shanghai Jiao Tong University, Shanghai 200240, China (e-mail: bjqin@sjtu.edu.cn; oo\_mhh@sjtu.edu.cn; m201812235@sjtu.edu.cn; junzhao@sjtu.edu.cn).

Yisong Lv is with the School of Continuing Education, Shanghai Jiao Tong University, Shanghai 200240, China (e-mail: yslv@sjtu.edu.cn).

Yueqi Zhu is with the Department of Radiology, Shanghai Jiao Tong University Affiliated Sixth People’s Hospital, Shanghai Jiao Tong University, Shanghai 200233, China (e-mail: zhuyueqi@hotmail.com).

Song Ding is with the Department of Cardiology, Ren Ji Hospital, School of Medicine, Shanghai Jiao Tong University, Shanghai 200127, China (e-mail: dingsong@renji.com).

Xu Chen is with the Center for Advanced Neuroimaging, University of California at Riverside, Riverside, CA 92521 USA (e-mail: xu.chen@ucr.edu).

Digital Object Identifier 10.1109/TMI.2022.3177626

## I. INTRODUCTION

Coronary artery disease (CAD) is a leading cause of death and disability worldwide. X-ray coronary angiography (XCA) is a standard method for diagnosing CAD. However, XCA images often suffer from low resolution, which makes it difficult to detect small vessels and their distal branches. Super-resolution (SR) techniques have been proposed to improve the resolution of XCA images. Robust principal component analysis (RPCA) is a popular method for SR in XCA. It decomposes the input image into a low-rank matrix and a sparse matrix, where the low-rank matrix represents the underlying vessel structure and the sparse matrix represents the background noise. However, RPCA is often computationally expensive and sensitive to initialization. In this paper, we propose a novel robust PCA unrolling network (RPCA-UNet) for SR in XCA. The proposed network is built upon a patch-wise spatiotemporal SR framework that is built upon a pooling layer and a convolutional long short-term memory network. The proposed network can not only gradually prune complex vessel-like artefacts and noisy backgrounds in XCA during network training but also iteratively learn and select the high-level spatiotemporal semantic information of moving contrast agents flowing in the XCA-imaged vessels. The experimental results show that the proposed method significantly outperforms state-of-the-art methods, especially in the imaging of the vessel network and its distal vessels, by restoring the intensity and geometry profiles of heterogeneous vessels against complex and dynamic backgrounds. The source code is available at <https://github.com/Binjie-Qin/RPCA-UNet>.

BC ( ) 9, CA

17. D 18

CA

(C) 19. CA

CA

B CA, C

1) A CA ( CA) CA

CA

CA

2) C CA

CA

CA

3) CA

BC ( ) 9, CA

## II. RELATED WORKS

### A. XCA Vessel Extraction

C 4, 5, 20, CA

21 CA

22 25

F 26

27

24, 25, 23

22

28 CA

29, 30 2D/3D 29, 31

An CA

32 CA

33, 34, C



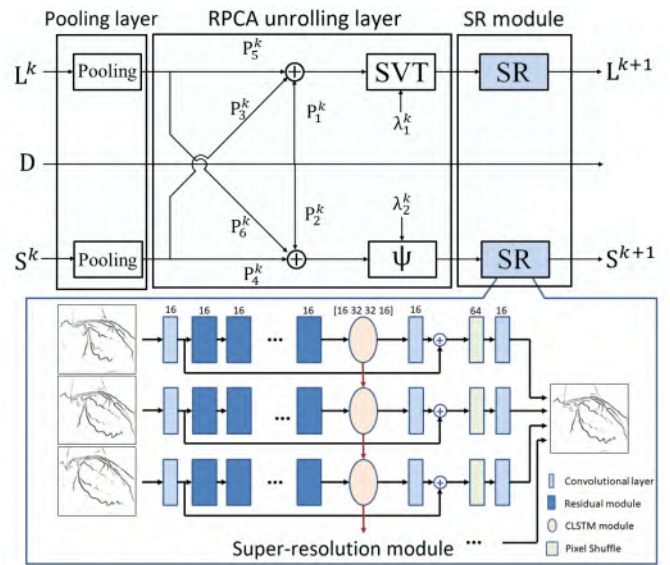


Fig. 1. The architecture of a single iteration/layer of RPCA-UNet for decomposing XCA data  $D$  into vessel ( $S$ ) and background ( $L$ ) components, which consists of a pooling layer, an RPCA unrolling layer, and an SR module. The SR module is mainly built upon the convolutional layer, residual module and CLSTM network.

$$D = L + S \quad (1)$$

A. RPCA Modelling

The RPCA model is used to decompose the XCA data  $D$  into vessel  $S$  and background  $L$  components. The RPCA model is defined as follows:

$$D = L + S \quad (1)$$

$$D = H_1 + H_2 \quad (2)$$

$$H_1 = H_2 = \dots$$

III. METHOD

CA-<sub>1</sub> n n F. . 1 n n CA

$$\frac{1}{2} \|H_1 - H_2\|_F^2 + \lambda_1 \|A\|_1 + \lambda_2 \|C\|_1 \quad (3)$$

$$\begin{bmatrix} H_1 \\ H_2 \end{bmatrix}, \begin{bmatrix} A \\ 0 \end{bmatrix}, \begin{bmatrix} 0 \\ A \end{bmatrix}, A, \begin{bmatrix} H_1 \\ H_2 \end{bmatrix} \quad (4)$$

$$\frac{1}{2} \|D - A\|_F^2 \quad (5)$$

$$\lambda_1 \|A\|_1 + \lambda_2 \|C\|_1 \quad (5)$$

$$\lambda_1 \left( \frac{1}{\lambda_1} H_1^H H_1 \right) + H_1^H H_2 + H_1^H D \quad (6)$$

$$\psi_{\lambda_2} \left( \frac{1}{\lambda_2} H_2^H H_2 \right) + H_2^H H_1 + H_2^H D \quad (7)$$

$$\lambda_1 \|A\|_1 + \lambda_2 \|C\|_1$$

**B. RPCA Unrolling Network**

$$\dots$$

$$\dots$$

$$\lambda_1 \|A\|_1 + \lambda_2 \|C\|_1 \quad (8)$$

$$\psi_{\lambda_2} \|C\|_1 + \lambda_2 \|C\|_1 \quad (9)$$

**C. Patch-Wise Super-Resolution Module**

... 67, ... 96





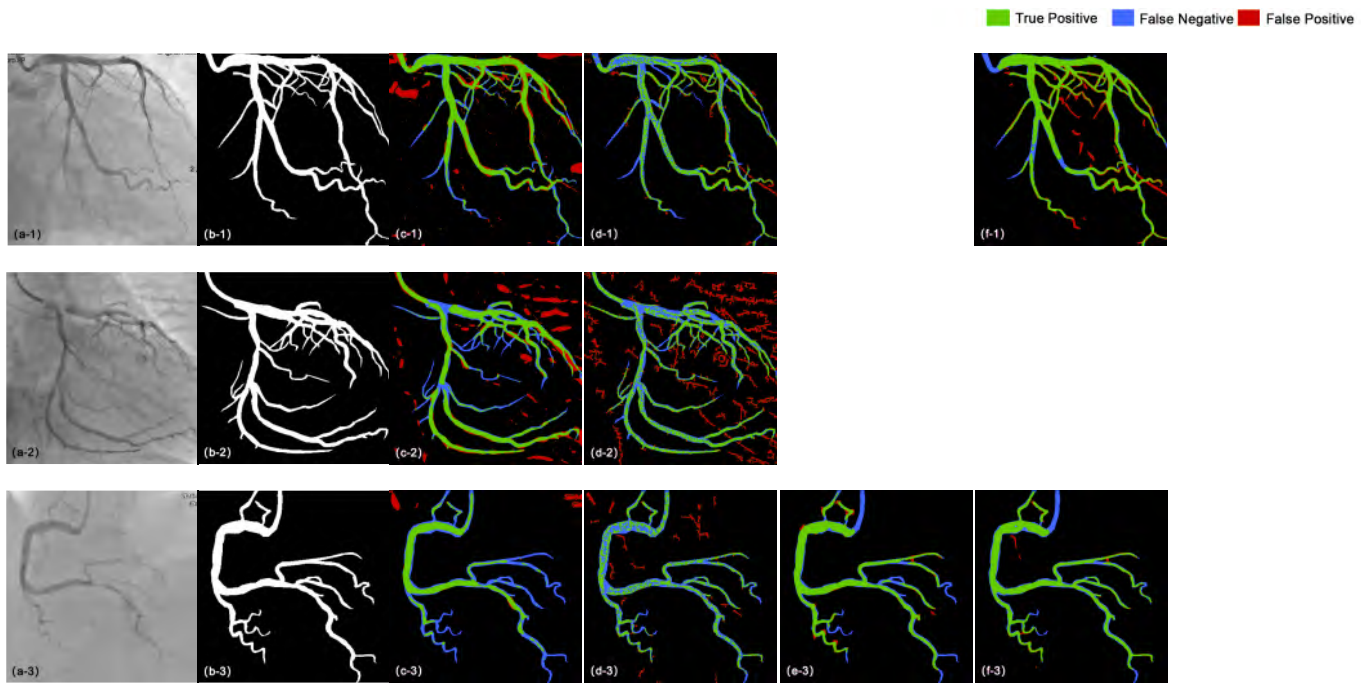


Fig. 3. XCA vessel segmentation results. Pixels labelled with green, blue, and red colours represent true positive pixels, false negative pixels, and false positive pixels, respectively. (a) Original XCA image; (b) Ground-truth vessel mask; (c) Frangi's; (d) Coyer's; (e) SVS-net; (f) CS<sup>2</sup>-Net; (g) RPCA-UNet.

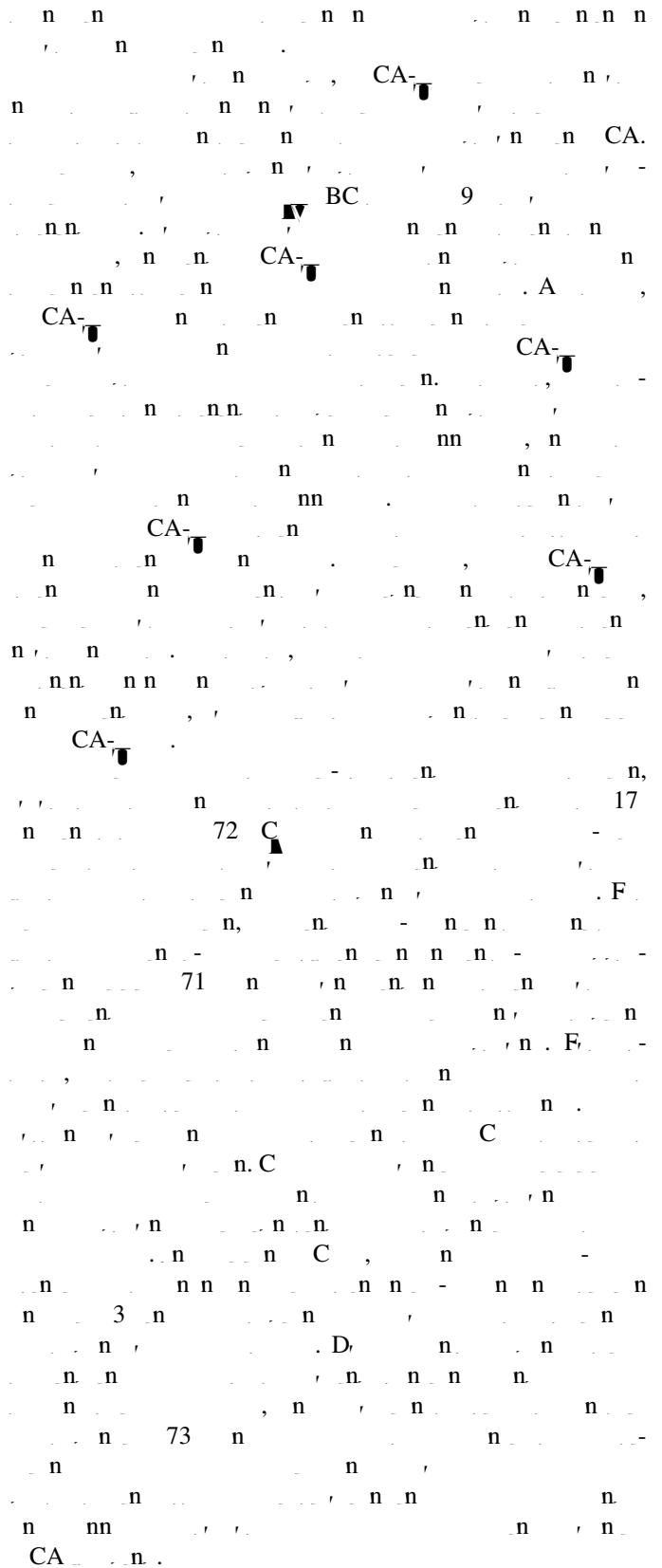
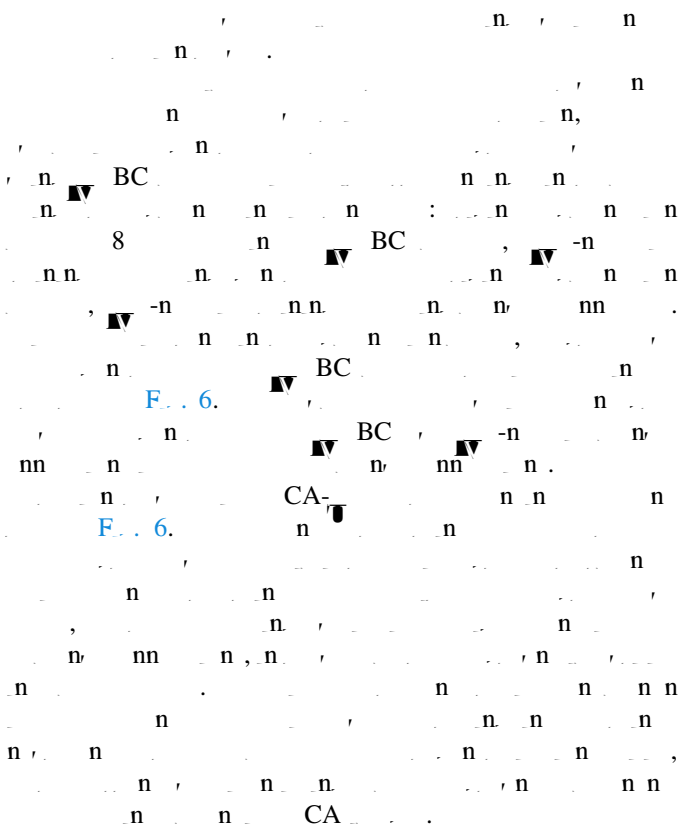
TABLE I

PERFORMANCE OF DIFFERENT VESSEL EXTRACTION METHODS  
IN TERMS OF CNR VALUES (MEAN STANDARD DEVIATION)





**Fig. 6.** The effect of coarse versus fine vessel label on the result of weakly supervised learning. The first row are the coarse and fine grey value labels automatically generated by the VRBC combined with different binary vessel mask segmentations, i.e. from left to right being original segmentation method in the VRBC, SVS-net with training data generated by the original segmentation method, SVS-net with training data by manual annotation; the second row of results are test cases of the corresponding networks trained with different grey value labels.



**V. CONCLUSION AND DISCUSSION**

CA-  
CA-  
CA-  
CA-  
CA-  
CA-  
CA-  
CA-  
CA-  
CA-

**ACKNOWLEDGMENT**

CA-  
CA-  
CA-  
CA-  
CA-  
CA-  
CA-  
CA-  
CA-  
CA-



47. F. N. et al., "A deep learning-based method for automatic detection of brain lesions in MRI scans," *IEEE Access*, vol. 6, pp. 44635–44643, 2018.
48. D. et al., "A deep learning-based method for automatic detection of brain lesions in MRI scans," *IEEE Access*, vol. 128, pp. 172–187, Apr. 2020.
49. et al., "A deep learning-based method for automatic detection of brain lesions in MRI scans," *IEEE Access*, vol. 68, pp. 102646, 2021.
50. et al., "A deep learning-based method for automatic detection of brain lesions in MRI scans," *IEEE Access*, vol. 198, pp. 105769, 2021.
51. et al., "A deep learning-based method for automatic detection of brain lesions in MRI scans," *IEEE Access*, vol. 40, no. 5, pp. 1329–1339, 2021.
52. C. et al., "A deep learning-based method for automatic detection of brain lesions in MRI scans," *IEEE Access*, vol. 69, pp. 3699–3713, 2021.
53. C. et al., "A deep learning-based method for automatic detection of brain lesions in MRI scans," *IEEE Access*, vol. 300, pp. 70–79, 2018.
54. B. et al., "A deep learning-based method for automatic detection of brain lesions in MRI scans," *IEEE Access*, vol. 5, no. 4, pp. 537–550, 1994.
55. et al., "A deep learning-based method for automatic detection of brain lesions in MRI scans," *IEEE Access*, vol. 42, no. 11, pp. 2960–2966, 2020.
56. et al., "A deep learning-based method for automatic detection of brain lesions in MRI scans," *IEEE Access*, vol. 50, pp. 158–167, 2019.
57. et al., "A deep learning-based method for automatic detection of brain lesions in MRI scans," *IEEE Access*, vol. 565, pp. 278–305, 2021.
58. et al., "A deep learning-based method for automatic detection of brain lesions in MRI scans," *IEEE Access*, vol. 51, no. 3, pp. 1747–1756, 2021.
59. A. et al., "A deep learning-based method for automatic detection of brain lesions in MRI scans," *IEEE Access*, vol. 183, pp. 115312, 2021.
60. et al., "A deep learning-based method for automatic detection of brain lesions in MRI scans," *IEEE Access*, vol. 183, pp. 115312, 2021.